Kitepower Ground Station

Modelling the Ground Station of the Kitepower System

I.P. Bakker

Bachelor Thesis Applied Mathematics TU Delft

TU Delft

Kitepower Ground Station

Modelling the Ground Station of the Kitepower System

by

I.P. Bakker

to obtain the degree of the Bachelor of Applied Mathematics
at the Delft University of Technology,
to be defended publicly on Friday July 13, 2018 at 12:00.

Student number:	4481941	
Project duration:	May 1, 2018 – July 13, 2018	
Thesis committee:	Dr. J.F.B.M. Kraaijevanger,	TU Delft, supervisor
	Prof. dr. ir. A.W. Heemink,	TU Delft
	Drs. E.M. van Elderen,	TU Delft
	Ir. P. Faggiani	Kitepower

An electronic version of this thesis is available at `http://repository.tudelft.nl/`.

TU Delft

Abstract

Kitepower is a start up that generates energy using kites. The Kitepower system consists of airborne components, and a ground station where a drum is connected to a generator/electrical motor. For generating energy a so called pumping cycle is performed. In a pumping cycle energy is generated during the traction phase when the kite pulls the drum, and some of this generated energy gets consumed during the retraction phase when the kite is reeled in. The net energy is stored in a rechargeable battery pack.

In this thesis a model and a control is derived for the ground station of the Kitepower system, for the purpose of making physically realistic simulations.
The Kitepower system is divided into a kite system and a ground station system. For the kite system already a proper quasi-steady model exists, but in order to do simple kite simulations and analyses a simplified version of this kite model is derived in chapter 3. In chapter 4 a ground station model is derived by using basic physical concepts and in chapter 5 a velocity and a force control are proposed for the ground station model.
The derived ground station model and controls are implemented with Python, and incorporated in the kitepower software in order to make simulations of a full pumping cycle.
In the result chapter 6 simulations are being done with and without using the ground station model. Both the proposed velocity and the force control are used for the simulations. The simulations are compared on physically realistic behavior and validated with experimental data.

Acknowledgement

First of all, I want to thank Hans Kraaijevanger for his help and support, and for sharing his enthusiasm for this research with me.

Furthermore, 10 years ago I joined the student boardsport society *SPIN* in Utrecht. *SPIN* was about kite surfing with a fantastic vibe. Most of my friends today I met during those wonderful years.
This thesis is about generating energy with kites, and the atmosphere I've experienced within Kitepower was very similar to the energetic *SPIN* vibe. I want to thank Kitepower for giving me this opportunity, and especially Pietro Faggiano who supervised me within Kitepower.

Contents

1

List of Symbols and Abbreviations

Table 1.1: Symbols and Abbreviations

Symbols and Abbreviation	Explanation
F_t	tether force
v_t	tether reeling velocity
r	radius of the drum
J	Moment of inertia of the ground station
τ_d	torque on the drum exerted by the tether
τ_t	torque on the axis exerted by the power transducer
τ_{fr}	torque on the axis caused by friction
ω	angular velocity of the ground station system
$\dot{\omega}$	angular acceleration of the ground station system
G_r	gear Ratio
$\mathbf{v}_a$	apparent wind velocity
$\mathbf{v}_w$	wind velocity
$\mathbf{v}_{k,r}$	radial kite velocity
$\mathbf{v}_{k,\tau}$	tangential kite velocity
ϕ	azimut angle kite
θ	elevation angle kite
ρ	air density
C_R	resulting aerodynamic force constant
QM	quasi-steady kite model
QMcomplex	quasi-steady kite model proposed by Vlugt et al. (2017)
QMsimple	simplified version of *QMcomplex*
GM	ground station model

2

Introduction

Kitesurfing is popular nowadays. The strong traction generated by the kite makes surfers go super fast in the water and enables them to make high jumps in the air. Kitesurfing is an exciting experience which makes it possible to play with the forces of nature. A nice thing about kitesurfing is that the kite is deflatable and fits in a rather small backpack. This makes it easy to travel and to bring the gear wherever in the world.
With kitesurfing the traction generated by the kite is directly converted into fun. But wouldn't it be possible to convert this traction into consumable energy? This is a question people have been asking themselves for quite a long time already. In the past, kites have been used for tasks such as aerial photography [3], lifting up the first radio antennae to suitable altitudes for reception of messages [4] and for meteorological observations. But it was only later that kite constructions were built for generating energy.
Nowadays kites are used for the propulsion of ships. This construction consists of flying a gigantic kite from the bow of a ship. The traction developed by the kite assists in pulling the merchant vessel through the water and therefore decreases the consumption of fuel of the ship [9].

Figure 2.1: Ship propulsion by Kite

This application is truly inspiring. However, it would also be interesting if the traction could be converted into consumable energy, so that it could function as a sustainable and environmental friendly energy resource. This is the topic the research group from the TU Delft of the former astronaut Wubbo Ockels has been working on. In 2016 Kitepower was founded as a result of the work from the research group. Kitepower is a leading start-up that develops an innovative and cost-effective Kitepower system, as an alternatives to existing wind turbines by using kites to generate electricity. Some advantages of the Kitepower system in comparison to the traditional wind turbines is that it uses 90% less material, it can harness stronger and more persistent winds at higher altitudes, and it's a relativaly lightweight and therefore mobile construction [6]. This reduces the cost of maintenance and makes it possible to generate electricity in remote locations.
Already in 2007, the first 20kW Kitepower system demonstrated the proof of concept. The 100kW system, which Kitepower is currently developing, will be one of the first airborne wind energy systems available on the market [6].

In the Kitepower system a kite is connected to a (winch)drum on the ground with a tether. This drum is connected to an electrical motor/generator, which we will refer to as a (power) transducer. This power transducer can function as a generator or as an electrical motor. During the reel-out phase the kite pulls the tether, which makes the tether reel out from the drum, and therefore spins the drum around. This phase is also called the *traction phase*. In this phase the power transducer is used as a generator and electricity is generated by converting the rotational movement of the drum. The generated traction is maximized by flying the kite in fast cross wind eight figure maneuvers and by powering the kite. Powering the kite means increasing its angle of attack, the angle at which the wind strikes the kite's surface [1]. The difference between a powered and a de-powered kite is demonstrated in figure 2.2a, where the red kite represents a powered kite and the blue one a de-powered kite.
When the maximum tether length is reached, the kite is de-powered by decreasing the angle of attack, and the tether is reeled in by the drum, using the power transducer as an electrical motor. This reel-in phase is also called the *retraction phase* and consumes some of the previously generated energy. Because of the power settings the traction phase generates a lot more energy than the retraction phase consumes, and therefore energy is generated throughout each cycle. A rechargeable batterypack is used to buffer the energy over the pumping cycles.
The traction and retraction phase are demonstrated in figure 2.2b. One cycle as described above is called a *pumping cycle* [11].

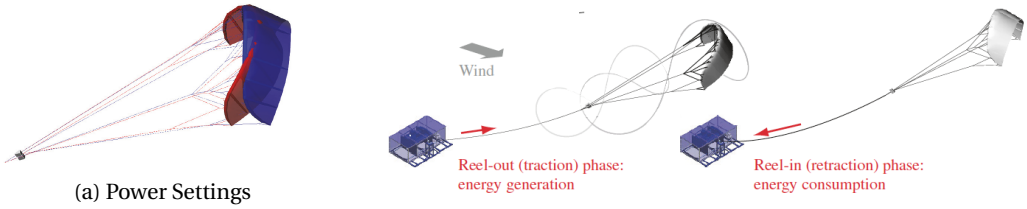

(a) Power Settings

(b) Traction and Retraction phase

Figure 2.2: Powersetting and phases of the kite

In the following sections one can read a more detailed description of the system design and its testflights. Then the Kitepower system will be split into two interacting systems to finally come to the research question and methodology.

2.1. System Design

The system conists of airborn hardware, a ground station and control software. The airborne hardware includes a kite and a Kite Control Unit (*KCU*), which essentially is a remote-controlled cable manipulator. The kite has an inflatable leading edge, similar to the kitesurf kites on the beach, and can vary in size.
The drum/generator module is responsible for traction power conversion while constantly monitoring and adapting the force in the tether. The control software includes two alternating autopilots, one for flying the figure eight maneuvers during tether reel-out and one for the reel-in phase [1]. The following figure shows all essential components of the Kitepower system of the earlier 20kW system, which is still representative for the 100kW system, except for the kite size.

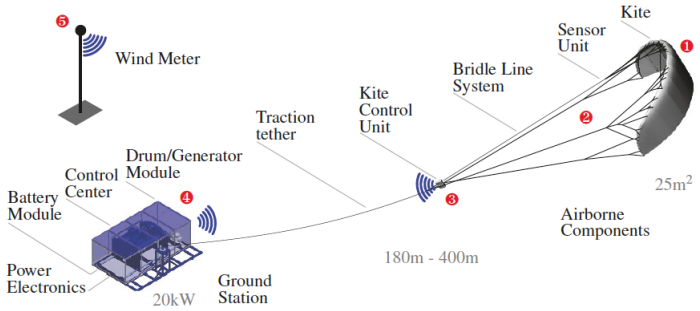

Figure 2.3: System Design

The wind meter is used to measure the reference wind velocity at a fixed altitude close to the ground. From this reference measurement, the wind velocity at higher altitudes can be predicted.
The quasi-steady behavior of the kite throughout a pumping cycle is well described in the paper *Quasi-Steady Model of a Pumping Kite Power System* by Vlugt et al. (2017) [11]. A brief overview of their derived kite model will be given in chapter 3. Since a detailed description of the kite is beyond the scope of this thesis, we will now focus on the ground station.
The ground station is a reliable and robust, but still mobile unit. It basically consists of a big drum with two power transducers on each side. In between the drum and the power transducer a gearbox is constructed with a fixed gear ratio. The following figure shows a picture of the ground station.

Figure 2.4: Picture of the Ground Station

A spooler distributes the line on one layer over the length of the drum. At the cable exit point in the spooler, the tether force can be measured. The tether is a strong but lightweight and flexible cable made of the polyethylene high performance fiber Dyneema®[1].

The generator stores energy in a rechargeable battery pack. The main battery is charged by the pumping operation of the kite. During the reel-in phase power is drawn from the main battery to pull back the kite. The net energy produced during such a cycle is enough to power all computers of the system and to charge the main battery. A future step could be to feed the obtained access power into the grid or make it available for an end user that is not connected to the grid [1].

In chapter 4 a model for the ground station will be derived. This model takes the tether force of the kite on the drum as input and calculates the reeling velocity of the tether. The ground station model takes the moment of inertia of the system into account as well as the friction, and the torque of the (power) transducer. The controllable element of the ground station, is the torque of the transducer. This torque can increase or decrease, and is controlled by the software. In section 5 controls of the model will be derived.

2.2. Test flights

The 100 kW Kitepower system is currently being developed. New features get tested every week during test flights. Test flight are on open fields, such as the Maasvlakte of Rotterdam Harbour or the former military airfield in Valkenburg, or sometimes in the wind tunnels at the TU Delft.
During test flights, measurement data is obtained for the purpose of improving the equipment and the models. The system is tested towards its limits, resulting sometimes in spectacular and unexpected situations and breaking records.

(a) Control Room (b) Test flight kite (c) Safety first

Figure 2.5: Test flight Valkenburg (May 2018)

2.3. Interacting Systems

The Kitepower system can be divided into two interacting systems:

1. the Kite system
2. the Ground Station (*GS*) system.

The interaction between those systems can graphically be represented as follows:

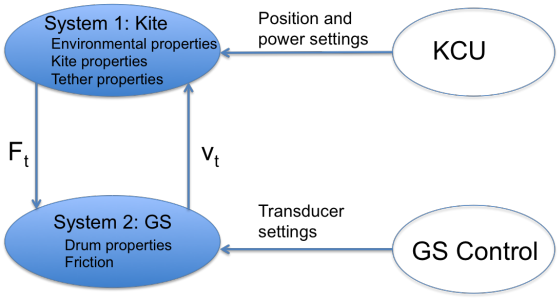

Figure 2.6: Interacting Systems

The kite system generates tether force (F_t) according to environmental, kite and tether properties. Environmental properties are for example the wind velocity and density at a certain altitude. Kite properties include the kite mass and aerodynamic lift and drag properties according to its shape and the tether properties consist of the tether length and mass. The kite system is controlled by the KCU, which steers the kite position and controls the power settings.
The tether force can be considered as an input for the ground station system, since it generates torque on the drum. This torque on the drum results in a reeling velocity (v_t) of the tether which is determined by the tether force, the drum properties (e.g. moment of inertia) as well as the friction in the system. It is controlled by torque settings of the transducer. The reeling velocity is an input for the kite system since it influences the generated traction. The tether force can be decreased by reeling out faster, or increased by reeling out slower, or even reeling in.

2.4. Research Question and methodology

The kite system is already modeled properly by Vlugt et al. (2017) [11], and implemented by Kitepower for the purpose of making simulations. In chapter 3 this model is described and simplified for analysis purposes. But for the ground station no model exists yet within Kitepower. For doing simulations, currently the reeling velocity is fixed to a certain value for each phase in the pumping cycle. There are no physical concepts incorporated in the ground station model yet. Therefore the research question of this thesis is:

> How can we mathematically model and control the Kitepower ground station in order to make physically realistic simulations?

The objective of this research is to derive a physically realistic ground station model and control, to predict the real life behavior of the ground station with simplistic computer models. To derive a ground station model, relevant physical concept are being used and combined. For deriving the control, control theory has been consulted and a simplified version of the kite model is derived to do analysis on the controls.

The derived model and the controls are implemented in Python and incorporated in Kitepowers software in order to make simulations of a full pumping cycle and to observe the physically realistic behavior of the simulation.

In the following chapters we will first discuss and simplify a quasi-steady kite model, then a physically realistic ground station model will be derived and finally two controls are proposed.
In the control chapter some simulations are made using the derived simplified kite model in order to observe the behavior of the control. In the chapter Results, chapter 6, one can find simulations of a full pumping cycle using Kitepower's kite model and the ground station model and controls derived in this thesis.

3

Model of the Kite System

Vlugt et al. (2017) [11] proposed a quasi-steady model of the kite system in their paper *Quasi-Steady Model of a Pumping Kite Power System*. This quasi-steady kite model will in this thesis be referred to as *QMcomplex* (Quasi-steady Model complex) and is implemented by Kitepower to predict the real life behavior of the kite during the pumping cycle. With this model realistic simulations of a full pumping cycle can be made. In the result chapter 6 simulations are being done using *QMcomplex*.
In order to make simple simulations of the ground station, and to do some analysis on the controls, a simplified version of the quasi-steady model, *QMsimple*, will be derived in this chapter. This model is based on *QMcomplex* but with some extra assumptions.

3.1. QMcomplex

The kite system simulation is not trivial, due to several reasons. The kite is for example flexible, which makes it hard to predict its aerodynamic properties. Also, in the pumping kite cycle the kite flies over a large altitude range, which complicates the environmental properties and affects the kites behavior. This is another reason why modeling the kite is hard.
Vlugt at al. (2017) made the following assumptions to the kite system:

1. the study is limited to kites with relatively large surface-to-mass ratio, so that the timescale of dynamic processes is generally very short compared to the timescale of typical maneuvers or complete pumping cycles. The kite responds therefore more or less instantaneously, which results in flight operations dominated by the balance of aerodynamic, tether and gravitational forces. It can therefore be approximated as a transition through *quasi-steady* flight states.

2. the analysis is limited to typical tether lengths, which are much larger than the geometrical dimensions of the kite, so that inertial forces such as centrifugal forces can be neglected.

3. the tether is assumed to be inelastic and represented by a straight line.

4. the aerodynamic properties of the kite are assumed to be constant throughout each phase.

5. the atmospheric properties are assumed to be constant over time.

With these assumptions the researchers developed two kite models, where in the first model the effect of gravity on the kite and the tether is neglected, and in the second model gravity is taken into account. Both models perform well when validated with experimental data, although the model with gravity taken into account performs best.
However, to do some easy analyses on the tether force and to make some plots throughout this report, we will now derive a simpler version of the quasi-steady model (*QMsimple*), taking the model of Vlugt et al. (2017) as a guideline.

3.2. QMsimple

For simplifying reasons the model without taking gravity into account will be taken as inspiration. When deriving *QMsimple* the most important aspects of the first quasi-steady model from Vlugt et al. (2017) will be highlighted.

To derive *QMsimple*, the following extra assumptions are made:

1. the wind velocity and the air density are assumed to be constant. This we will denote as follows: $v_w = v_w^*$ and $\rho = \rho^*$.
2. the position of the kite is in *QMcomplex* determined by spherical coordinates (r, θ, ϕ). In the simplification the kite is assumed to be aligned with the wind direction. So in the wind frame, which can be seen in figure 3.1, the azimut angle (ϕ) is considered constant zero. Therefore the tangential component of the kite velocity $(v_{k,\tau})$ is also considered 0, so the kite velocity only has a radial component $(v_{k,r})$. Furthermore the elevation angle (θ) is assumed to be fixed (θ^*).

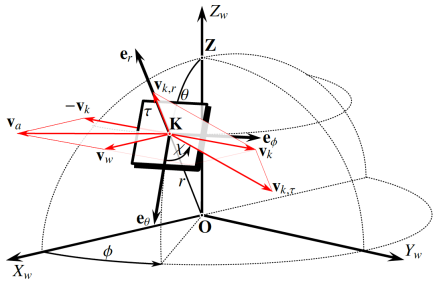

Figure 3.1: Wind frame and decomposition of the kite velocity

Vlugt et al. (2017) describe the apparent wind velocity $(\mathbf{v}_a)$, the wind velocity relative to the kite, as follows:

$$\mathbf{v}_a = \mathbf{v}_w - \mathbf{v}_k.$$

and when decomposed in all spherical coordinates the following description appears,

$$\mathbf{v}_a = \begin{bmatrix} \sin\theta\cos\phi \\ \cos\theta\cos\phi \\ -\sin\phi. \end{bmatrix} v_w - \begin{bmatrix} 1 \\ 0 \\ 0 \end{bmatrix} v_{k,r} - \begin{bmatrix} 0 \\ \cos\chi \\ \sin\chi \end{bmatrix} v_{k,\tau} \tag{3.1}$$

In this simplified situation the kite velocity (v_k) only has a radial component, so

$$\mathbf{v}_a = \mathbf{v}_w - \mathbf{v}_{k,r}.$$

When plugging in the assumptions $(v_w = v_w^*, \phi = 0, \theta = \theta^*, v_{k,\tau} = 0)$ the apparent wind velocity vector can be described as follows:

$$\mathbf{v}_a = \begin{bmatrix} \sin(\theta^*) \cdot v_w^* - v_{k,r} \\ \cos(\theta^*) \cdot v_w^* \\ 0 \end{bmatrix} \tag{3.2}$$

And therefore magnitude of the apparent wind velocity squared equals

$$v_a^2 = (\sin(\theta^*) \cdot v_w^* - v_{k,r})^2 + \cos(\theta^*)^2 \cdot v_w^{*^2}. \tag{3.3}$$

3. The next assumption is that the tether is a straight line, and the effect of sagging due to distributed gravitational loading is not taken into account. This implies that the radial kite velocity is identical with the reeling velocity which is controlled by the ground station

$$v_{k,r} = v_t = r \cdot \omega \tag{3.4}$$

with r the radius of the drum and ω the angular velocity of the drum. And so

$$v_a^2 = (\sin(\theta^*) \cdot v_w^* - r\omega)^2 + \cos^2(\theta^*) \cdot v_w^{*^2} \tag{3.5}$$

From this equation one can see that the angular velocity (ω) is the only variable that can influence the apparent wind velocity. All other variables are fixed.

4. The last assumption for *QMsimple* is that also the projected surface area of the kite (S), the area the apparent wind is projected on, is considered to be constant.

   From Vlught et al. (2017) [11] it is known that the tether force can be calculated as

$$F_t = \frac{1}{2}\rho C_R v_a^2 S, \tag{3.6}$$

   where C_R is the constant resulting aerodynamic force coefficient which is the magnitude of the drag and lift coefficient, C_L, C_R respectively. In the simplified model $\rho = \rho^*$ and $S = S^*$ both constant, so by defining

$$\alpha = \frac{1}{2}\rho^* C_R S^*$$

   $\alpha > 0$ is a constant. This will simplify equation (3.6) to

$$F_t = \alpha v_a^2. \tag{3.7}$$

When combining all assumptions described above and substituting equation (3.5) for the apparent velocity, the final shape of the Quasi-Steady Model (*QMsimple*) arises:

$$\boxed{F_t = \alpha((\sin(\theta^*) \cdot v_w^* - r\omega)^2 + (\cos(\theta^*) \cdot v_w^*)^2)} \tag{3.8}$$

This simplified model is a function that is determined only by the angular velocity, with a fixed wind velocity and elevation angle.
Let $\beta = \sin(\theta^*) \cdot v_w^*$ and $\gamma = \alpha(\cos(\theta^*) \cdot v_w^*)^2$, then $\beta > 0$ and $\gamma > 0$ are both constants. When substituting this, *QMsimple* can be simplified to

$$\boxed{F_t = \alpha(\beta - r\omega)^2 + \gamma} \tag{3.9}$$

In the following sections *QMsimple* will be used to do analyses on the tether force, and to derive a velocity and force control.
In the simulations of the result chapter 6, the advanced *QMcomplex* will be used.

4

Model of the Ground Station

In this chapter a model for the ground station will be derived using physical concepts. In appendix A, the basic physical concepts relevant for deriving the model are briefly explained. We will first look at all the components of the ground station and see how these physical concepts are applicable on these components. Finally the model is derived by combining all physical concepts of the components.

A picture of the Kitepower ground station can be seen in section 2.1. In order to derive a model of the ground station, the design is abstracted in the following figure.

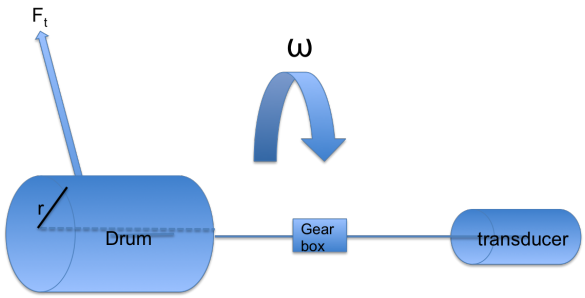

Figure 4.1: Ground Station Schematic

An explanation of the symbols can be found in the list of symbols and abbreviations, chapter 1. The arrows of the angular velocity point in the direction which we define to be the positive rotational direction of the system. During the traction phase the system will rotate in this direction, and so there is a positive angular velocity. During retraction the rotation is in opposite direction and the angular velocity will then be considered negative.
This schematic representation is a simplification of the actual ground station. The two motors/generators are combined in one (power) transducer, the electrical system of the transducer is not shown and also the battery is dismissed in this drawing. The motivation for this simplification is that the aim is to make a ground station model that can simulate physically realistic *mechanical* behavior. Therefore the detailed electrical influences on the system are beyond the scope of this thesis.

For deriving the model, the following assumptions are made:

1. We assume F_t pulls in tangential direction with respect to the rotation motion, and it pulls right from the drum. This is quite realistic, since the spool in front of the drum measures the applied force F_t and takes the elevation angle into account. This spool also fixes the tether exit point tangential to the rotational motion of the drum.

2. The mass of the drum, and therefore the moment of inertia (J) is assumed to be constant. We neglect the fact that the moment of inertia changes due to the mass of the tether when it is reeled on or off, since the

mass of the drum is much greater than that of the lightweight Dyneema®tether.

3. The radius of the drum (r) is assumed to be constant. In fact the radius changes when tether is reeled on or off the drum, but the spool in front of the ground station distributes the line on one layer over the length of the drum. Since the tether would only increase the radius of the drum with 1.6 %, this influence is negligable.

The leading physical concept for the model is the conservation law of angular momentum, equation (A.3):

$$J\dot{\omega} = \tilde{\tau}_{net} \tag{4.1}$$

where J is the moment of inertia of the system, and τ_{net} is the sum of all torques. In this system torque is applied by the drum, friction and the transducer. This leads to the following basic model:

$$J\dot{\omega} = \tilde{\tau}_d + \tilde{\tau}_{fr} + \tilde{\tau}_t \tag{4.2}$$

Where $\tilde{\tau}$ stands for the torque on the drum side on the system. This will be explained in more detail in section 4.4.
In the upcoming sections these torques and the influence of the gearbox on them will be described and mathematically modeled. According to the assumptions, the radius and mass of the drum are constant, and therefore also the moment of inertia of the drum is fixed. The rest of the system also has a fixed moment of inertia, and therefore we consider J to be constant in time.

4.1. The drum

First we focus on the torque of the drum. The following figures show a schematic representation of the drum and a full body diagram on which all the forces on the drum are depicted.

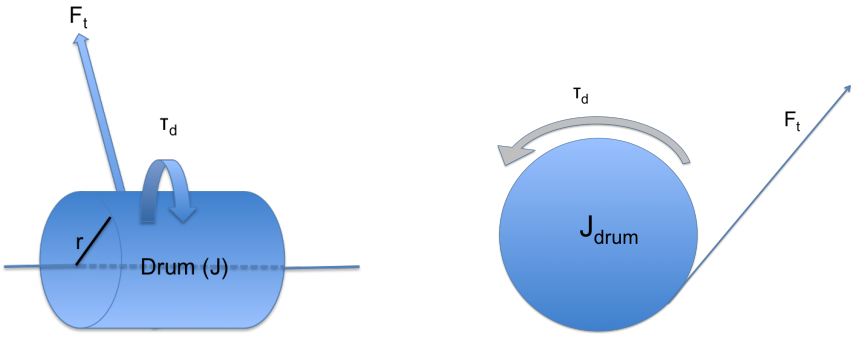

(a) Drum schematic (b) Full Body Diagram Drum

Figure 4.2: Drum

On the drum there is an external force applied by the tether force in tangential direction with respect to the rotational motion. This makes the drum to apply torque in the positive direction. From equation A.1 it follows that the torque of the drum equals:

$$\tilde{\tau}_d = F_t r \tag{4.3}$$

When applying the conservation law of angular momentum only on the drum, the following equation arises.

$$J\dot{\omega} = F_t r \tag{4.4}$$

By integrating the angular acceleration, we find the angular velocity for the drum

$$\omega = \frac{r}{J}\int_0^t F_t(\hat{t})\,d\hat{t}. \tag{4.5}$$

To research the behavior of the angular velocity of only the drum, we've plotted the angular velocity of several tether force profiles. This results in the following plots where in every subplot the upper figure represents the tether force profile and the lower plot the corresponding velocity profile.

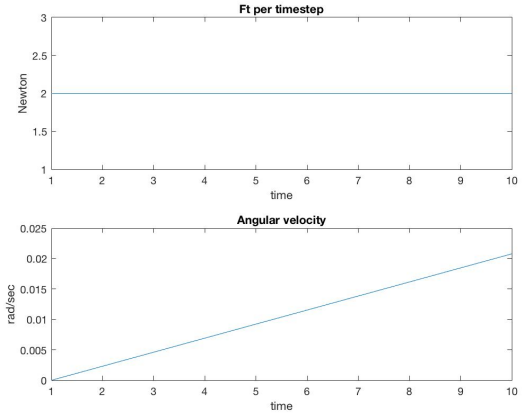

(a) constant tether force

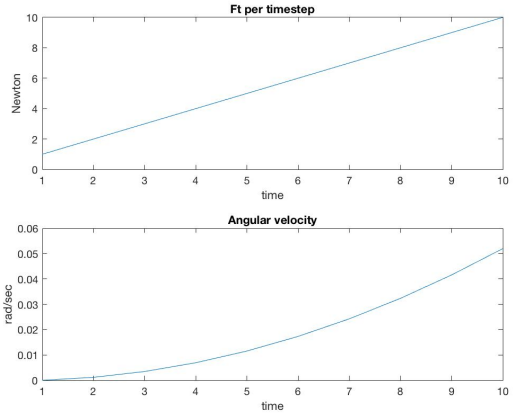

(b) linearly increasing tether force

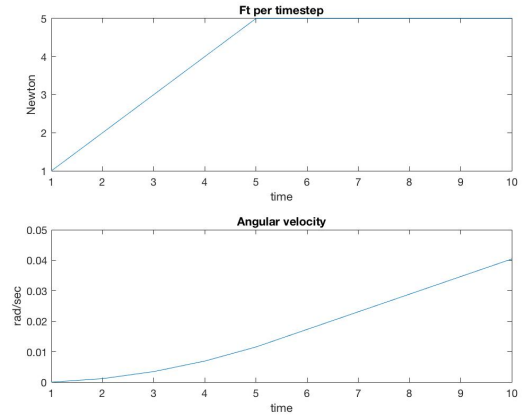

(c) linearly increasing to constant tether force

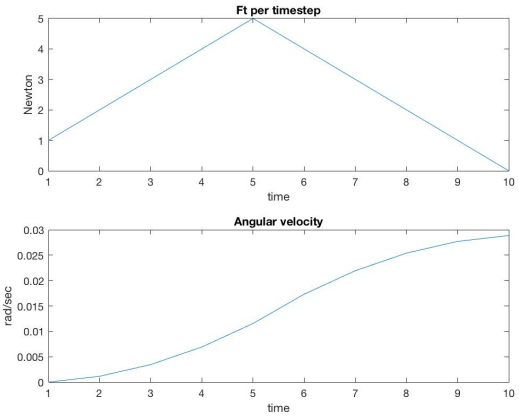

(d) linearly increasing-decreasing tether force

Figure 4.3: Force profiles with corresponding angular velocity of the drum

It is clear that a constant tether force profile leads to a linear velocity profile (subfigure a), and a linearly increasing tether force profile leads to a quadractically increasing velocity profile (subfigure b), as to be expected from equation 4.5. A combination of those tether profiles also leads to a combination of these velocity profiles, as to be seen in subfigures c and d.
Note that in these simulations the tether force is set to a certain profile. This is not very realistic since the tether force is usually determined by the kite system which is influenced by the external forces, such as the wind velocity, and the reeling velocity. Changing the reeling velocity also changes the tether force profile.

4.2. Friction

Friction is an unwanted force in the system because it only generates heat and no electricity. The aim is to keep the friction as small as possible. However, friction occurs in several places in the system. For example, in the ball bearing of the axis and in the gearbox. Friction can be seen as a damper, and can therefore be modeled as a torque in the opposite to the angular velocity [10]. If the angular velocity is in positive direction, the friction torque is in negative direction and vice versa. This is depicted in the following figure:

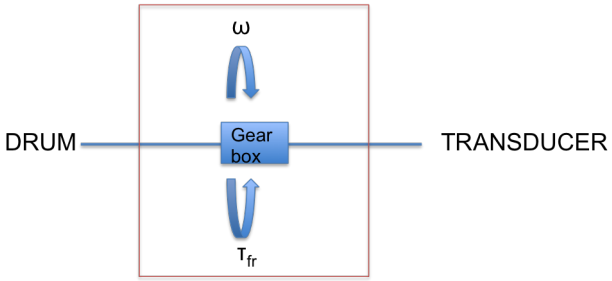

Figure 4.4: Friction Schematic

The net friction torque (τ_{fr}) is the sum of all the friction torques in the system. From appendix A follows that the friction is linear with the angular velocity, therefore we model the friction as follows:

$$\tau_{fr} = -\hat{b}\omega. \tag{4.6}$$

where $\hat{b} > 0$ is a fixed constant that needs to be determined for the system.

4.3. Transducer

We will now focus on the (power) transducer. A transducer is a device that converts energy from one form to another (Wikipedia). In the ground station, the (power) transducer can either function as a generator or as an electrical motor. Both the generator and the electrical motor are rather complicated electrical systems that are beyond the scope of this thesis. But, in the software of the ground station it is possible to set the torque of the transducer to a certain value, and to increase and decrease the torque during the operation by acting on the winding of the machine. Although the transducer is actually advanced, this possibility of setting the torque with software simplifies the situation.

The torque of the transducer appears in two different ways:

1. Torque due to the generation of energy. The generation of energy causes a resistance to the angular velocity of the drum. The external force of the transducer torque is in this case the resistive force to this rotational motion. Note that the magnitude of the generator torque will therefore never be greater than the drum torque, since it is a resistive torque.

2. Torque generated by the electrical motor. In this situation the external force, is the force applied by the motor.

We define the positive direction of the transducers torque opposite to the positive direction of the drum torque. This is due to the fact that during reel-out phase, when the torque of the drum is in positive direction, the torque of the transducer will be in opposite direction in order to generate energy. Generating energy is the main objective of the kitepower system, and therefore we define this to be the positive transducer torque direction. This is depicted in the following figure:

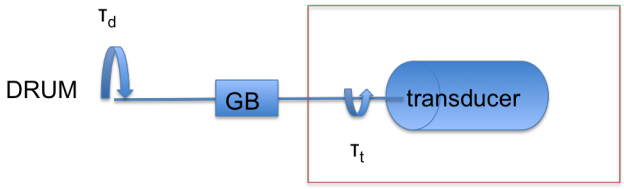

Figure 4.5: Transducer Schematic

Where *GB* stands for GearBox. Since the transducer torque is positively defined in the direction opposite to the drum torque, the transducer torque will be modeled as $-\tau_t$. When neglecting the gear ratio, which will be

described in following section, this results in the following net torque of the total system:

$$\tau_{net} = \tau_d + \tau_{fr} - \tau_t. \tag{4.7}$$

This leads to the following equation of the conservation of angular momentum (still neglecting gear ratio)

$$J\dot{\omega} = \tau_d + \tau_{fr} - \tau_t. \tag{4.8}$$

The transducer torque is not always in opposite direction to the drum torque. One can see that increasing τ_t contributes to decreasing the angular acceleration, and vice versa. When during reel-out the reeling velocity should increase (for example to control the tether force during a wind gust), the transducer can contribute in this acceleration by lowering the resistive generator torque or even applying a torque in the same direction as the drum torque. In the last case the transducer applies a negative torque, and should switch from generator to electrical motor.
When going from the reel-out to the reel-in phase the transducer should apply a positive torque greater then $\tau_d + \tau_{fr}$ in order to make the angular acceleration negative and the angular velocity to decrease and go to a negative reel-in velocity. In this situation the transducer should also function as an electrical motor, since the external force of the transducer should be greater than the external force caused by the rotational motion of the drum. This can only be achieved by applying an electrical motor torque in positive direction. To be able to satisfy both electrical motor applications described above, the electrical motor should be able to apply torque in both directions. Luckily the ground station is advanced enough!

For further research it would be interesting to investigate the transducer torque in more detail. For now we just assume that we can set the torque, but in fact the transducer torque is generated by a more complex electrical system.

4.4. The gearbox

In this subsection the focus will be on the systems behavior due to the gearbox.

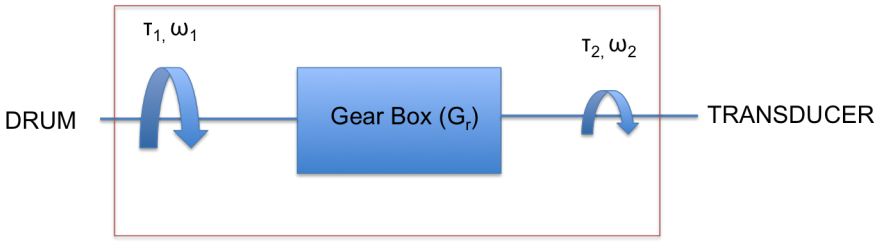

Figure 4.6: GearBox Schematic

In figure 4.6, τ_1, ω_1 represent the torque and angular velocity *on the drum side* of the gearbox, and τ_2, ω_2 the torque and angular velocity *on the transducer side* of the gearbox. In the current ground station the gear ratio (G_r) is fixed. In this ratio the gear connected to the transducer is considered to be the driver gear, and the drum gear the driven gear. From the physical concepts, equation A.8 now follows for the angular velocity:

$$\omega_2 = G_r \omega_1. \tag{4.9}$$

For the torque the following holds according to equation A.10

$$\tau_2 = \frac{1}{G_r} \tau_1. \tag{4.10}$$

Since the variable of interest is the reeling velocity of the tether, we're interested in the angular velocity and net torque *on drum side* of the gear box. This net torque is influenced by the drum, the friction and by the transducer torque. Let $\tilde{\tau}_d$, $\tilde{\tau}_{fr}$ and $\tilde{\tau}_t$ be the drum, the friction and the transducers torque on the drum side respectively.
In section 4.2 we defined τ_{fr} as the sum of all friction torques in the system. To calculate the friction torque on

the drum side of the system, the friction torque on the transducer side should be multiplied with the gear ratio. This results in the following model of the frictions torque on the drum side:

$$\tilde{\tau}_{fr} = -b\omega_d \tag{4.11}$$

where b is the fixed constant, with the correct magnitude when measured on the drum side.

The set transducer torque also needs to be multiplied with the gear ratio in order to get the transducer torque on the drum side of the system. And therefore

$$\tilde{\tau}_t = -G_r\tau_t. \tag{4.12}$$

Now alle the torques on the drum side required to derive the ground station model, are known.

4.5. Full model of ground station

In the previous section, all separate components of the ground station are modeled which led to the following conclusions:

$$\begin{aligned} \tilde{\tau}_d &= F_t r && (4.13)\\ \tilde{\tau}_{fr} &= -b\omega && (4.14)\\ \tilde{\tau}_t &= -G_r\tau_t. && (4.15)\\ & && (4.16) \end{aligned}$$

We saw that the net torque is the sum of all torques, and therefore the net torque can be modeled as:

$$\tilde{\tau}_{net} = F_t r - b\omega - G_r\tau_t. \tag{4.17}$$

For the reel-out phase, we find the following full body diagram.

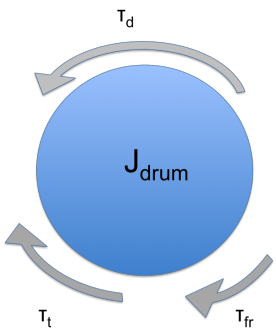

Figure 4.7: Full Body Diagram during reel-out phase

The final step is to derive the full model of the ground station. When substituting equation(4.17) in the equation of the law of conservation of the angular momentum the full model arises.

$$\boxed{J\dot{\omega} = F_t r - b\omega - G_r\tau_t.} \tag{4.18}$$

This is the final model will be used to make physically realistic simulations of the ground station.

5

Controlling the ground station

During a pumping cycle it is sometimes desirable to control the reeling velocity or the tether force. Control on the reeling velocity is needed so that the power load can be controlled. Controlling the tether force is necessary in order to prevent the system from breaking. For example, in a strong wind gust, a lot of force is generated in the kite that causes a lot of tension in both the tether and the kite. Reeling out faster will decrease this force, which in turn will reduce the tension. This is why a *velocity control* and a *force control* is needed for the ground station throughout a pumping cycle.
The reeling velocity can be controlled at the ground station by acting on the transducer torque. Changing the reeling velocity also affects the tether force generated by the kite. This means that at the ground station, both the velocity and the tether force can be controlled by changing the settings of the transducer torque.
In order to emphasize that the transducer torque settings are the control objective, we will refer to the transducer torque as u from now on in the equations.

$$G_r \tau_t = u,$$

which changes the ground station model to

$$J\dot{\omega} = F_t r - b\omega - u. \tag{5.1}$$

When we want to apply control we can either use an open-loop technique or a closed-loop technique. In an open-loop control the system is controlled in a pre-described manner, according to a desired reference value [10]. According to this reference value, a control can be derived, causing the desired output to the system by the process. The open-loop configuration is given in the figure below.

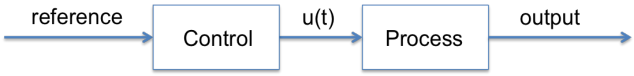

Figure 5.1: open-loop control

In an open-loop control, the actual state of the system has no influence on the control value. In a closed-loop control however, the control value is determined by the error (e) of the reference value and the measured output. In every feedback loop, the measured output is used as feedback. This is shown in the following figure

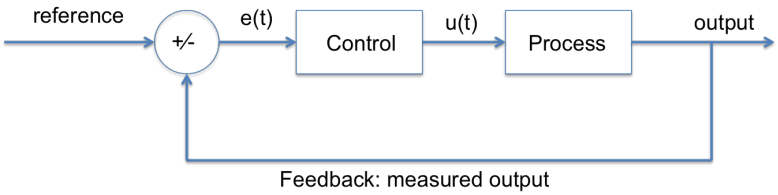

Figure 5.2: closed-loop (feedback) control

Let $r(t)$ be the reference value and $y(t)$ the measured output, then the error is defined as follows:

$$e(t) = y(t) - r(t). \tag{5.2}$$

We will first derive an open-loop control for the ground station by making use of *QMsimple*. Then, closed-loop controls will be derived using a more intuitive approach.
A disadvantage of the open-loop control is that the latter is derived from a simplified kite model (*QMsimple*) and therefore doesn't respond correctly in the advanced situation. The closed-loop control, however, does because of the feedback that it receives. Therefore only the closed-loop controls are implemented in the Kitepower system and used in the results section.

5.1. Open-loop control, using *QMsimple*

In this section an open-loop control will be derived using *QMsimple*.
Remember that for *QMsimple* holds:

$$F_t = \alpha(\beta - r\omega)^2 + \gamma, \tag{5.3}$$

with α, β and γ constants. If we plug this equation into the ground station model, the following differential equation arises:

$$J\dot{\omega} = r(\alpha(\beta - r\omega)^2 + \gamma) - b\omega - u. \tag{5.4}$$

Before the control is derived, we will first prove that, under certain conditions, the model has two stationary points (ω_1^* and ω_2^*) when the transducer torque is set to a fixed value. After this, we will show that only one of those stationary points is stable. This implies that a fixed transducer torque together with taking the right reference and initial values, will make the angular velocity converge to a stationary value.
Once this is proven, we will determine the value of the control that is needed, so that the angular velocity or force converges to a desired reference value. This will result in an open-loop velocity and force control of which the convergence will be discussed.

We will now show that for a fixed transducer torque, the ground station model has two stationary points (ω_1^* and ω_2^*). Therefore we define:

$$p(\omega) = r(\alpha(\beta - r\omega)^2 + \gamma) - b\omega, \tag{5.5}$$

here $p(\omega)$ is a second order polynomial. Since both $r, \alpha > 0$, the second order term is greater then zero and $p(\omega)$ is a parabola with a minimum.
Let $u = u^*$ be a fixed transducer torque. Then, for the stationary points in the ground station model the following equation must hold:

$$r(\alpha(\beta - r\omega)^2 + \gamma) - b\omega = u^*, \tag{5.6}$$

and so

$$p(\omega) = u^*. \tag{5.7}$$

Figure 5.3 shows sketches of the three possible combinations of $p(\omega)$ and u^*.
The arrows on the u^* axis in the sketches represent the phase line of $\dot{\omega}$. If $\dot{\omega} > 0$, ω increases and the arrows will point to the right, and vice versa.

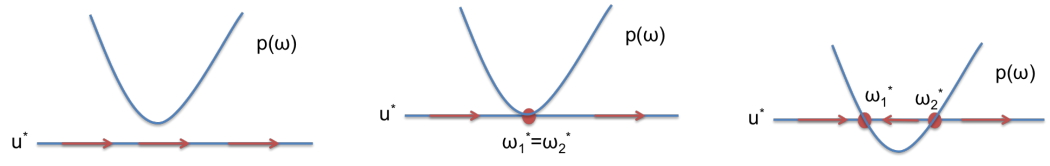

(a) No stationary points (b) One stationary point (c) Two stationary points

Figure 5.3: Possible situations for stationary points

1. In the situation in figure 5.3a, $u^* < p(\omega)$ for all $\omega \in \mathbb{R}$. From the ground station model it now follows that $\dot{\omega} > 0$ for all $\omega \in \mathbb{R}$ and no stationary point exists.

2. In the situation in figure 5.3b, $u^* = p(\omega)$ for only one $\omega \in \mathbb{R}$. This means that there is only one stationary point, $\omega_1^* = \omega_2^*$. From the phase line however, it is clear that this point is not stable.
3. In the situation in figure 5.3c, $u^* = p(\omega)$ for two $\omega \in \mathbb{R}$, meaning there are two stationary points ω_1^* and ω_2^*. It can be seen from the phase line that only the lowest stationary point, ω_1^*, is stable.

If we now calculate the stationary points of the ground station model, one finds that:

$$\omega_{1,2}^* = \frac{2\alpha\beta r^2 + b \pm \sqrt{4\alpha\beta b r^2 + 4\alpha r^3(u^* - r\gamma) + b^2}}{2\alpha r^3} \tag{5.8}$$

From the square root in the equation, it follows that a stationary point ($\in \mathbb{R}$) exists if and only if

$$4\alpha\beta b r^2 + 4\alpha r^3(u^* - r\gamma) + b^2 \geq 0. \tag{5.9}$$

This gives the following condition for u^*:

$$u^* \geq \frac{-(4\alpha b\beta r^2 + b^2)}{4\alpha r^3} + r\gamma. \tag{5.10}$$

From the analogy used in the sketches in figure 5.3, it follows that the only *stable* stationary point is

$$\omega_1^* = \frac{2\alpha\beta r^2 + b - \sqrt{4\alpha\beta b r^2 + 4\alpha r^3(u^* - r\gamma) + b^2}}{2\alpha r^3}, \tag{5.11}$$

under the condition that

$$u^* > \frac{-(4\alpha b\beta r^2 + b^2)}{4\alpha r^3} + r\gamma. \tag{5.12}$$

From this it can be concluded that when the transducer torque (u^*) is fixed to a suitable value, ω will converge to a stationary point, if for the initial value holds that:

$$\omega(0) \in (-\infty, \omega_2^*). \tag{5.13}$$

Knowing that the angular velocitiy will converge if the transducer torque is fixed, yields the possibility to derive a closed loop velocity and force control by setting the transducer torque such that the velocity converges to a *desired* value.

5.1.1. Open-loop velocity Control

Suppose we want the angular velocity to converge to a certain reference velocity ω^{vref}.
Then setting

$$u^{vref} = r(\alpha(\beta - r\omega^{vref})^2 + \gamma) - b\omega^{vref}, \tag{5.14}$$

makes the value of ω converges to the stationary point (ω^*), such that

$$r\alpha(\beta - r\omega^*)^2 - b\omega^* - r\alpha(\beta - r\omega^{vref})^2 - b\omega^{vref} = 0. \tag{5.15}$$

This equation holds if and only if

$$\omega^* = \omega^{vref}.$$

From this, it follows that setting the transducer torque to this value will cause the following desired convergence:

$$\lim_{t\to\infty} \omega(t) = \omega^{vref}.$$

This equation only holds under the conditions that $\omega(0) \in (\infty, \omega_2^*)$ and:

$$\omega^{vref} < \frac{2\alpha\beta r^2 + b}{2\alpha r^3}. \tag{5.16}$$

Under these conditions, the open loop velocity control, such that ω converges to ω^{vref}, is defined as follows:

$$\boxed{u_v^* = r(\alpha(\beta - r\omega^{vref})^2 + \gamma) - b\omega^{vref}}. \tag{5.17}$$

5.1.2. Open-loop force control

Suppose we want F_t to converge to a certain reference force (F_t^{Fref}). In that case, we actually want ω to converge to a certain reference velocity (ω^{Fref}) such that

$$r(\alpha(\beta - r\omega^{Fref})^2 + \gamma) = F^{Fref}. \tag{5.18}$$

Since this is a quadratic equation, the equations has two solutions:

$$\omega_{1,2}^{Fref} = \frac{1}{r}\Big(\beta \pm \sqrt{\frac{F^{Fref} - r\gamma}{r\alpha}}\Big). \tag{5.19}$$

As $r(\alpha(\beta - r\omega^{Fref})^2 + \gamma)$ is again a parabola with a minimum, it follows, using the same analogy from the sketches in figure 5.3, that the only possible stable stationary velocity is equal to:

$$\omega_1^{Fref} = \frac{1}{r}\Big(\beta - \sqrt{\frac{F^{Fref} - r\gamma}{r\alpha}}\Big). \tag{5.20}$$

Since we want F_{Fref} to converge to a steady state, we pick ω_1^{Fref} as the desired angular velocity value.

From here on, the deriviation is analogous to the velocity control. Setting the transducer torque to the following value:

$$\boxed{u_F^* = r(\alpha(\beta - r\omega_1^{Fref})^2 + \gamma) - b\omega_1^{Fref}} \tag{5.21}$$

will make the velocity converge to the desired value, when the conditions for ω^{Fref} are taken into account as well.

5.1.3. Convergence of the open-loop control

In this section we will look at the convergence speed when $\omega \approx \omega^{vref}$. In this situation we can make use of a linearization. Let ω^{vref} be the desired angular velocity and let

$$u_v^* = r(\alpha(\beta - r\omega^{vref})^2 + \gamma) - b\omega^{vref}$$

be the control. For

$$J\dot{\omega} = r(\alpha(\beta - r\omega)^2 + \gamma) - b\omega - u_v^*, \tag{5.22}$$

it follows that

$$J\dot{\omega} = -(2r^2\alpha\beta + b)(\omega - \omega^{vref}) + r^3\alpha(\omega^2 - \omega^{vref^2}). \tag{5.23}$$

When it is assumed that $\omega \approx \omega^{vref}$, ω^2 can be linearly approximated by only looking at the first order term of the Taylor expansion:

$$\omega^2 \approx 2(\omega - \omega^{vref})\omega^{vref} + \omega^{vref^2}. \tag{5.24}$$

Plugging this linearization into equation 5.23, it follows that:

$$J\dot{\omega} = -(2r^2\alpha\beta + b - r^3\alpha\omega^{vref})(\omega - \omega^{vref}). \tag{5.25}$$

Let z be the difference: $\omega - \omega^{vref}$, then $\dot{z} = \dot{\omega}$. This leads to the following differential equation

$$J\dot{z} = -(2r^2\alpha\beta + b - r^3\alpha\omega^{vref})z \tag{5.26}$$

Solving this differential equation analytically gives the following result:

$$z = e^{-\frac{1}{J}(2r^2\alpha\beta + b - r^3\alpha\omega^{vref})t} z(0). \tag{5.27}$$

From this result it is clear that $\lim_{t\to\infty} z = 0$ and therefore that indeed $\lim_{t\to\infty} \omega = \omega^{vref}$, when

$$\omega^{vref} < \frac{2\alpha\beta r^2 + b}{2\alpha r^3}. \tag{5.28}$$

The convergence speed is determined by the fixed values r, α, β, b and ω^{vref} and cannot be influenced by the actual state of the system.
This open-loop control is derived from the simplified model, *QMsimple*. Further research is needed to extend this control to a open-loop control that is useful for the Kitepower system.

5.2. Closed-loop (feedback) control

In this section we will propose closed-loop (feedback) controls by making use of an intuitive approach. The controls defined in this section will be applicable for the Kitepower system, since the feedback will force the control to act until it reaches the desired reference value.
In closed-loop control theory it is most common to look at a *PID control*, where the P, I, and D stand for Proportional, Integral, Derivative respectively [7][10]. In a *PID* control the value of the control is determined by the error (e) between the reference value of the control variable and the measured output. If we define u^{ref} as a reference control value, for example the open-loop control value we've derived in the previous section, the overall control function of a *PID* control can be mathematically expressed as

$$u(t) - u^{ref} = \lambda_p e(t) + \lambda_i \int_0^t e(\tilde{t}) d\tilde{t} + \lambda_d \frac{de(t)}{dt}, \tag{5.29}$$

where λ_p, λ_i and λ_d are constants for the proportional, integral and derivative term respectively. To create a smooth feedback control all three terms in the control function play a role. However, it is also possible to only use a proportional control, an integral control or other combinations.
The open-loop control derived in the previous section could be converted to a feedback control by adding a proportional component for example. This would result in the following control

$$u(t) - u^{ref} = \lambda_p e(t). \tag{5.30}$$

A big advantage of a feedback control over a closed-loop control is that the convergence speed can be influenced by changing the values of λ.
However, for the derivation of a control for the advanced Kitepower system, the actual value of u^{ref} is unknown, since the open-loop feedback control derived in previous section was based on *QMsimple* and not on *QMcomplex*. In order to avoid this problem, integral controls are being used to control the ground station. The integral control is defined as follows:

$$u(t) - u^{ref} = \lambda_i \int_0^t e(\tilde{t}) d\tilde{t}. \tag{5.31}$$

When taking the derivative on both sides with respect to the time, we find that:

$$u'(t) = \lambda_i e(t). \tag{5.32}$$

The derivative shows that u^{ref} is not needed for the integral control. Therefore, integral controls are useful as they are capable of controlling the ground station model without knowing the value of u^{ref}. In a closed loop control, the control value is updated after every feedback cycle. Let u_k and u_{k+1} be the control values in feedback loop k and $k+1$ respectively, and $h = t_{k+1} - t_k$ the size of the time step, then discretizing the integral control (equation (5.32)), using explicit Forward Euler, will lead to the following updating formula:

$$u_{k+1} = u_k + h \cdot \lambda_i e_k. \tag{5.33}$$

In section 6.1 the explicit Forward Euler method will be briefly explained.

5.2.1. Integral velocity control

We will now derive a closed-loop integral velocity control by analyzing the desired behavior of the control.
The aim of the velocity control is to let the (angular) velocity converge to a certain reference value (ω^{ref}). When controlling the angular velocity, the latter should increase if $\omega < \omega^{ref}$, decrease when $\omega > \omega^{ref}$ or maintain a constant velocity when $\omega = \omega^{ref}$. All three situations will be discussed by making use of the ground station model.

1. Let's first discuss the situation where $\omega < \omega^{ref}$ and the objective is to increase ω. In order to increase ω, we must have that: $\dot{\omega} > 0$. This implies that:

   $$J\dot{\omega} = F_t r - b\omega - u > 0,$$

   since $J > 0$. The equation above holds if u small enough, so it makes sense if u is decreased.

2. In the situation where $\omega > \omega^{ref}$ and the objective is to decrease ω, the following equation must hold: $\dot{\omega} < 0$. This implies that
$$J\dot{\omega} = F_t r - b\omega - u < 0.$$
The inequality above can be achieved by increasing u.

3. Finally, when $\omega = \omega^{ref}$, the objective is to maintain ω. Therefore the following equation must hold: $\dot{\omega} = 0$. This implies that
$$J\dot{\omega} = F_t r - b\omega - u = 0.$$
To achieve this, u should be equal to
$$F_t r - b\omega.$$

For the velocity control, the error is equal to $\omega - \omega^{ref}$ and the desired velocity control described above can be obtained using the following integral velocity control rule:

$$\boxed{u_{k+1} = u_k + h \cdot \lambda_v(\omega - \omega^{ref})} \tag{5.34}$$

where $\lambda_v > 0$ is a constant that can be set by the control.
It can be seen that this control rule indeed follows the desired behavior; when $\omega < \omega^{ref}$ then u decreases and vice versa. When $\omega = \omega^{ref}$, u remains constant. However, $\dot{\omega}$ might not be zero (for example when $u \neq F_t r - b\omega$). In that case the angular velocity will still change and situation 1 or 2 will occur again in the next feedback cycle, which causes the control to respond. Because of this phenomenon, the control might oscillate towards its desired velocity. The gain λ_v will determine the strength of the control. A larger value of λ_v makes the control react quicker compared to a smaller λ_v. This is depicted in the following plots.

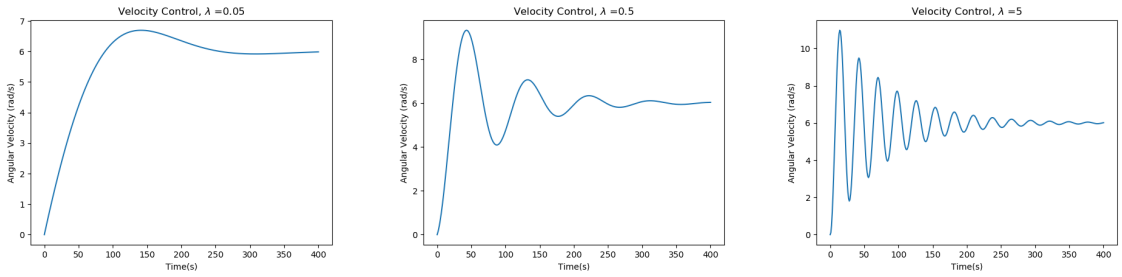

Figure 5.4: Effect of λ using velocity control

In these plots *QMsimple* is used to calculate the force and the objective of the control is to converge to $\omega^{ref} = 6$. It is clear from these plots that λ_v influences the convergence speed of the control, which was not possible with the open-loop control. One can see that the control for $\lambda_v = 0.05$ is the slowest converging control, but it oscillates and overshoots less compared to the larger values for λ_v. The higher the λ_v value, the quicker the control reacts, but at the same time it is also more unstable.

5.2.2. Integral force control

The objective of a force control is to let the tether force converge to a certain reference force (F_t^{ref}). When we look at *QMsimple* ($F_t = \alpha((\sin(\theta^*) \cdot v_w^* - r\omega)^2 + (\cos(\theta^*) \cdot v_w^*)^2)$), the tether force is determined by the wind velocity (v_w), the elevation angle (θ) and the reeling velocity ($r\omega$). The wind velocity and elevation angle are external forces that cannot be controlled by the ground station. The reeling velocity, however, can be controlled by fixing the transducer torque (u), just as in the case when we derived the velocity control.
It is clear from *QMsimple* that increasing the angular velocity (ω) decreases the tether force. So when the force is too strong, due to for example a gust, a solution to reduce the tether force would be to increase the reeling velocity. On the other hand, one can see that decreasing $r\omega$ implies that the tether force is increased. This means that when the tether force is too low, the reeling velocity should decrease as well.
In the force control the error is defined as: $F_t - F_t^{ref}$. In order to get the desired behavior of the control the following integral control rule is proposed:

$$\boxed{u_{k+1} = u_k - h \cdot \lambda_F(F_t - F_t^{ref})} \tag{5.35}$$

where $\lambda_F > 0$ is a constant that can be set by the control. It can be seen that this rule indeed follows the desired behavior; when $F_t > F_t^{ref}$, the transducer torque decreases and vice versa.
Again λ_F determines the reaction speed of the control. This can be seen in the following plots for several λ_F changes. The tether force is calculated by *QMsimple* and the reference force F_t^{ref}=1500.

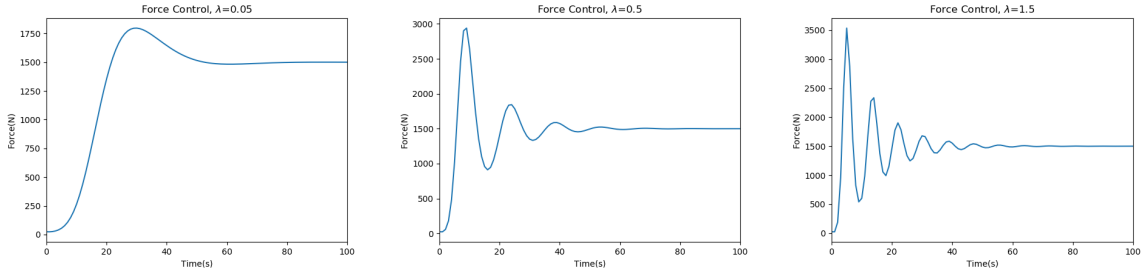

Figure 5.5: Effect of λ using force control

From the figures above it can be seen that also for the force control we have that the higher the value of λ_F is, the quicker the control reacts with a higher overshoot and due to the fast reaction the oscillation behavior occurs. A lower λ_F results in a slower control, but converges almost as quick without oscillating.

These oscillations in both the velocity and force control are not ideal when one wants to generate energy. Adding a Proportional and a Derivative component to the *PID controller* would most likely improve the control. This would a good topic for further research.

6

Results and Validation

In previous chapters a simplified version of the kite model, a ground station model and a control is derived. In these chapters *QMsimple* is being used for simulations of the ground station model and its controls.
In this chapter simulations of the ground station model will be performed for a full pumping cycle, using *QM-complex*, the quasi-steady kite model described in Vlugt et al. (2017).
For the implementation the models are discretized, calculating the new states for every time step. Let $\omega_k, (F_t)_k$, $(u_v)_k, (u_F)_k$ be the angular velocity, the tether force and the velocity and force control value at time step k respectively, and ω_{k+1} be the angular velocity at the next time step $k+1$, then the implementation cycles are depicted in the flow diagrams in figure 6.1. The velocity and the force control both need different inputs, resulting in different flow diagrams.

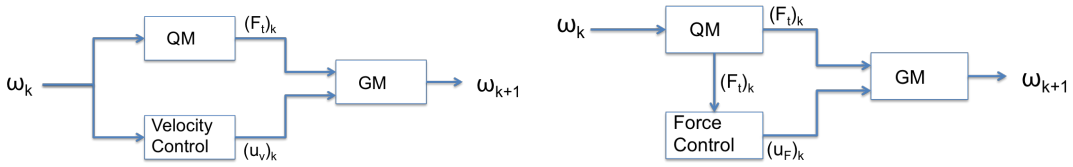

(a) Implementation with velocity control

(b) Implementation with force control

Figure 6.1: Implementation flow diagrams

In the implementation cycle the following steps are taken:

1. According to the reeling velocity (ω_k) the tether force $(F_t)_k$ gets calculated by the Quasi-steady kite Model (*QMcomplex*).

2. From the velocity or the tether force, the generator torque $(u_v)_k$ or $(u_F)_k$ will be determined by the velocity or force control respectively.

3. From $(F_t)_k$ and $(u_v)_k$ or $(u_F)_k$ the ground station model (*GM*) calculates the reeling velocity for the next time step (ω_{k+1}).

We will now briefly discuss the discretization of the ground station model. Then experimental data will be shown and simulations will be performed of a full pumping cycle, using *QMcomplex*.

6.1. Discretization of the ground station model

For the discretization of the ground station model the (explicit) Forward Euler method is being used. This method will be briefly outlined in this section.
Remember, the ground station model is the following:

$$\dot{\omega} = \frac{1}{J}(rF_t - b\omega - u). \tag{6.1}$$

Let t_k be the kth time value. We define the timestep $h = t_{k+1} - t_k$.
From the definition of a derivative it is known that

$$\dot{\omega} = \lim_{h \to 0} \frac{\omega(t+h) - \omega(t)}{h}. \tag{6.2}$$

For a small timestep h we approximate the differential equation of the basic model with the following difference equation:

$$\dot{\omega} \approx \frac{\omega_{k+1} - \omega_k}{h}. \tag{6.3}$$

In the (explicit) Forward Euler method all the values that are used to calculate the approximation at the new time value are already known. When applying the approximation of the derivative to the ground station model, while only using values of the previous time value, the following equation arises

$$\frac{\omega_{k+1} - \omega_k}{h} \approx \frac{1}{J}(r(F_t)_k - b\omega_k - u_k). \tag{6.4}$$

Let $\tilde{\omega}$ be the numerical version of ω it follows from previous equation that

$$\tilde{\omega}_{k+1} = \tilde{\omega}_k + \frac{h}{J}(r(F_t)_k - b\omega_k - u_k). \tag{6.5}$$

This discretization will be used in the implementation to update the angular velocity for every timestep when using the ground station model.

6.2. Results: experimental data and simulations of a full pumping cycle

In this section simulations are performed of a full pumping cycle using *QMcomplex*, the quasi-steady kite model as proposed by Vlugt et al. (2017) [11]. In order to be able to discuss the physically realistic behavior of the simulations, we will first look at experimental data of one pumping cycle. Then a simulation will be performed without using the derived ground station model, but instead using basic velocity settings. This method was being used to make simulations before.
Then a simulation will be made using the ground station model and the (closed-loop) velocity control, and finally a simulation will be made using the derived ground station model and the (closed-loop) force control.
All simulations will be compared on physically realistic behavior, using the current model with the basic settings as a baseline situation.

In the plots the pumping cycle will start with the retraction phase, then a transition phase, and finally the traction phase. The transition phase is needed to steer the kite in the correct position to start the traction. In the traction phase the path is modeled and therefore simulated as a straight line, as to be seen in figure 6.2, although in real life the kite will make figure eight maneuvers. However, in the experimental data these movements will be visible, since they cause a fluctuation in tether force, velocity and apparent wind velocity.

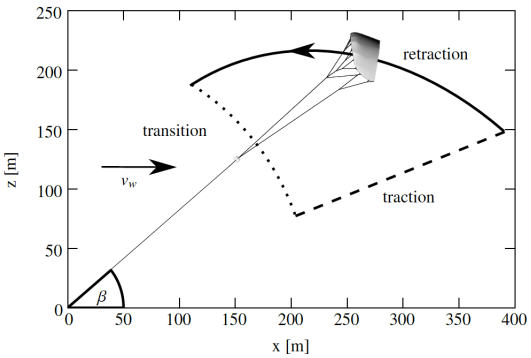

Figure 6.2: Pumping Cycle path

During the retraction phase and the first part of the transition phase, the kite is reeled-in, and during the second part of the transition phase and in the traction phase, the kite is reeled-out.

The retraction phase starts at the maximum tether length and continues until it reaches a set reference length. Then the cycle starts the transition phase, which is divided in two parts; in the first part the kite still reels-in, but it will slow down. Once the reeling velocity is zero, the second part of the transition phase starts and the kite will reel-out due to new kite settings. When a certain set elevation angle is reached, the transition phase stops and the traction phase starts. This phase continues until the tether length reaches its maximum.

From the experimental data and from the simulations, the following plots are produced:

1. The reeling velocity of the tether (m/s) over time. For positive values the kite is reeled-out, for negative values the kite is reeled-in.
2. The tether length (m) over time. The length represents the length of the tether in the air, so not on the drum. Since the simulation starts with the retraction phase, the tether length is at its maximum when the simulation starts. When the drum switches from reel-in to reel-out the tether length reaches its minimum for that cycle.
3. The tether force (kgf or N) over time. In different phases throughout the pumping cycle different power settings are being used, resulting in different forces. During the retraction phase the kite is de-powered, resulting in lower traction forces, and during the traction phase the kite is powered. In real life, the kite makes figure eight maneuvers during the traction phase for increasing the tether force. This increase in traction force is taken into account in the kite settings, but that path is not simulated. Also, the instability in the tether force, due to this trajectory in the traction phase, is not taken into account. However, in the experimental data the fluctuations in tether force during the traction phase can be observed.
4. The apparent wind velocity (m/s) over time. The apparent wind velocity is the flow velocity relative to the kite, which can be influenced by power settings, reeling velocity and steering maneuvers.
5. The path of the kite determined in in X-Z coordinates (comparable to the path in figure 6.2). In these plots the ground station is located in the origin and the axes represent the deviation of the kite from the ground station in the x and z direction in meters. Here z is the vertical direction, and x is the horizontal aligned with the wind direction.

In the experimental data, no plot will be available of the path. And in the simulations, no plot will be available of the apparent wind velocity.

All plots consist of 3 sections, divided by a cyan dashed line, representing the three phases:

1. retraction phase
2. transition phase
3. traction phase

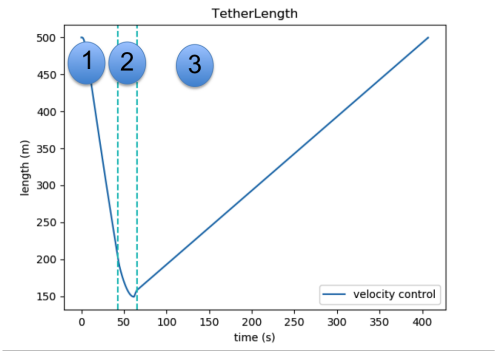

Figure 6.3: Three Phases

6.2.1. Experimental data

Since we will focus on physically realistic behavior of the simulations we will first discuss one pumping cycle of experimental data. The following plots show the experimental data of one pumping cycle of a test flight.

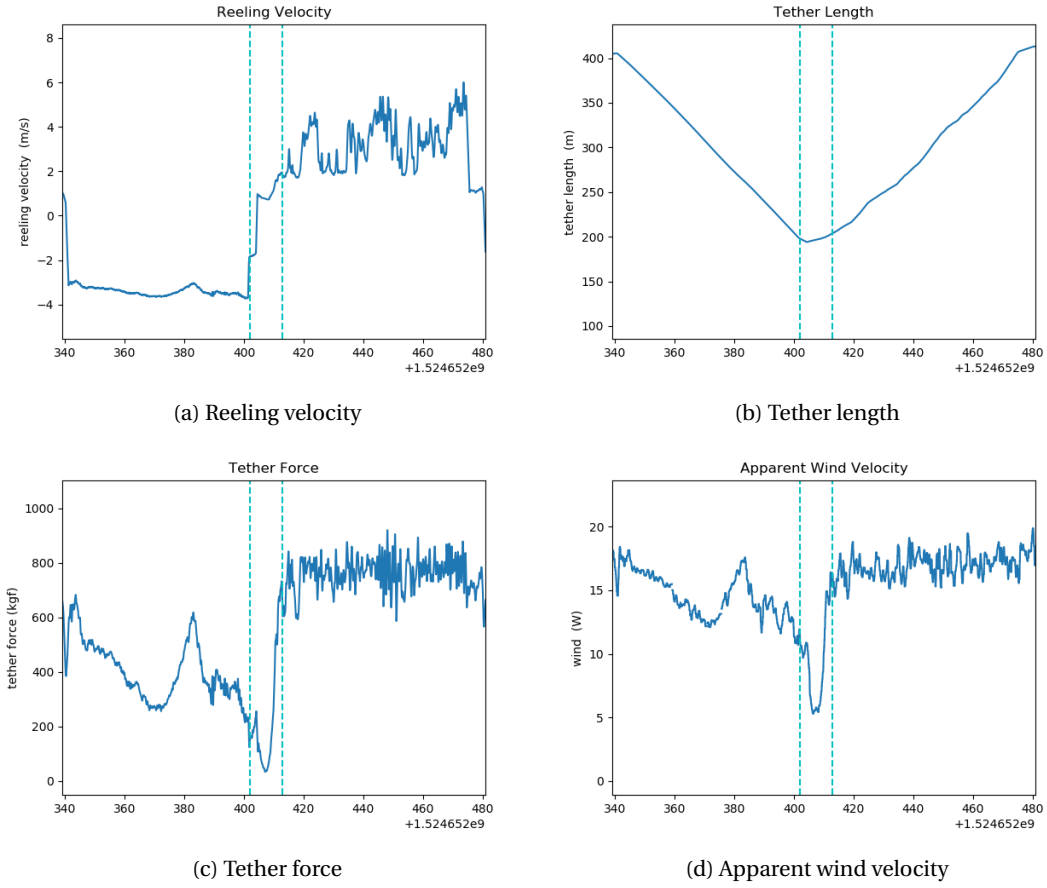

(a) Reeling velocity

(b) Tether length

(c) Tether force

(d) Apparent wind velocity

Figure 6.4: Experimental data

When looking at the retraction phase (1), one can see in subfigure 6.4a that the reeling velocity is quite stable throughout this phase. A small peak is caused by an increase of the apparent wind velocity. This reeling velocity results in a linearly decreasing trend in the tether length during the retraction phase as to be seen in subfigure 6.4b. Subfigure 6.4d shows that the apparent wind also has a decreasing trend. This is caused by the de-powered settings of the kite during the retraction phase, by decreasing the angle of attack with the wind. De-powering results in a lower apparent wind velocity, but reeling-in the kite generates some. Because of the decrease in apparent wind, also the tether force has a decreasing trend in the retraction phase, subfigure 6.4c.

In the transition phase (2) one can observe a quick increase in the reeling velocity. In the beginning of the transition phase the reeling speed is still negative, and therefore the tether length still decreases. The apparent wind velocity, and therefore the tether force drops, probably caused by the high acceleration of the reeling velocity.
In the second part of the transition phase the reeling velocity is positive and the tether length increases. The kite gets powered and starts its first traction maneuver, creating an increase in the apparent wind velocity and in the tether force.

During the traction phase (3) the kite makes fast cross wind maneuvers. This results in a quick change in tether force and in apparent wind velocity. Although the force varies quickly, one can observe a constant overall trend in the tether force during this phase. Due to the quick changes in the tether force, the torque on the drum varies a lot, resulting in a dynamic reeling velocity profile. Therefore also the linear increasing trend of the tether length is a bit more unstable.

We will now look at the simulations of a pumping cycle, and see how they compare to the experimental data on physically realistic behavior. For the simulation no plots will be shown of the apparent wind velocity. Instead plots of the kite path will be shown.

6.2.2. Simulation without ground station model

In the first simulation a pumping cycle is performed without using the ground station model. The simple settings that are now applied to the simulation are the following:

- a fixed reeling velocity of -7 m/s during the retraction phase,
- a fixed reeling velocity of 1 m/s during the transition and traction phase.

These settings result in the following plots:

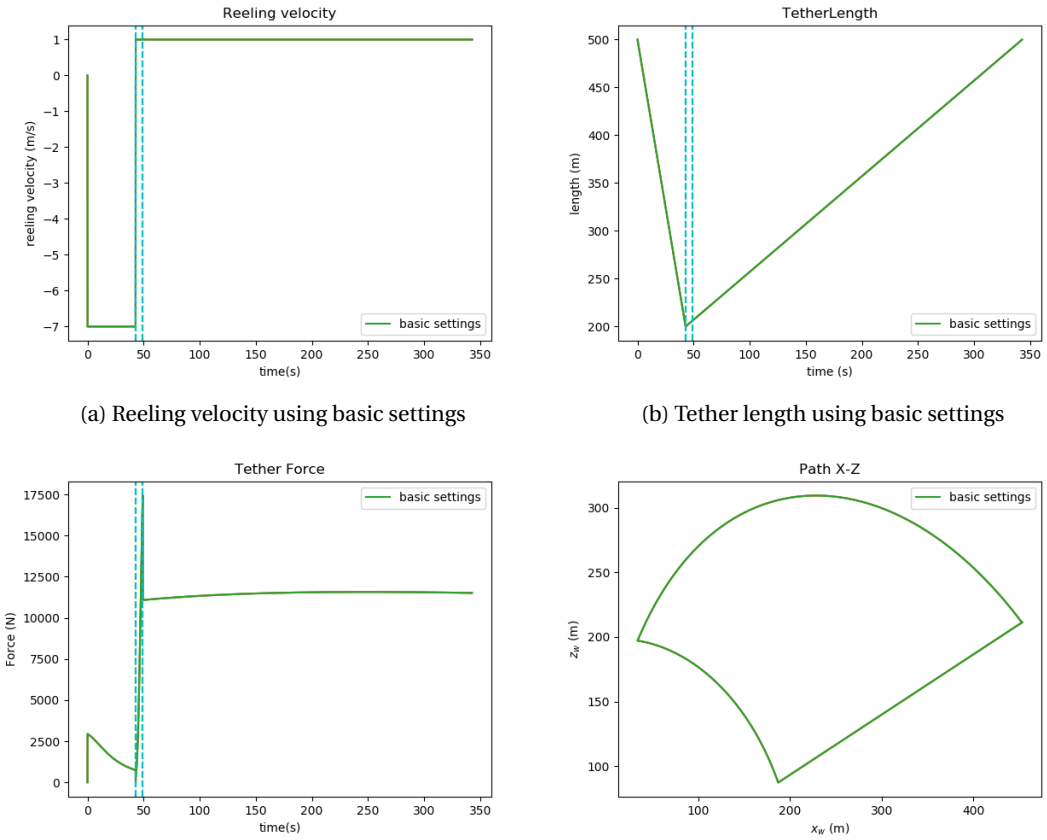

(a) Reeling velocity using basic settings

(b) Tether length using basic settings

(c) Tether force using basic settings

(d) Path using basic settings

Figure 6.5: Simulation of a full pumping cycle, using basic settings

The simple settings of the reeling velocity are plotted in the first subfigure 6.5a. It is clear from this plot that these settings are not physically realistic, since the acceleration between reel-in and reel-out is infinite. This implies that, for example, no moment of inertia of the system is taken into account.
The tether length can be observed in subplot 6.5b. According to the fixed reel-in and reel-out velocity, the tether length decreases and increases linearly respectively. The sudden switch between the angular velocity during reel-in and reel-out, causes a sharp, non smooth, turn around in the tether length. When comparing this to the tether length of the experimental data one can see that this turn around should be more smooth.
In subplot 6.5c the tether force can be observed. One can see that during the reel-in phase the tether force has a decreasing trend, just like the experimental data. In the transition phase, the sudden switch in angular velocity causes a high peak in the tether force. This is not desirable, and also not physically realistic when comparing it to the experimental data. During the traction phase the tether force converges to a steady state, which is

physically realistic.
The last subfigure, subfigure 6.5d, shows the simulated path of the kite. Sharp transitions between the phases can be observed, comparable to figure 6.2.

The most striking differences in this simulation, in comparison to the experimental data, is this sudden change in reeling velocity. This causes an unrealistic tether length profile and a high peak in the tether force. A better ground station model hopefully improves these aspects of the simulation.

6.2.3. Simulation using the ground station model and velocity control

In the following simulations the ground station model and the derived controls are incorporated in the Kitepower software and connected to *QMcomplex*. One simulation is performed using the (closed-loop) velocity control, and one simulation using the (closed-loop) force control, as proposed in chapter 5. The λ values of both the velocity and force control are found by trial and error.

In the following simulation, using the (closed-loop) velocity control, the reference reeling velocity is set to -7 m/s during the retraction phase and 1 m/s during the traction phase. In the transition phase the reeling velocity will have a reference velocity 0 in the first part, and when it reaches this velocity the kite will change power settings and the new reference velocity is 1m/s.

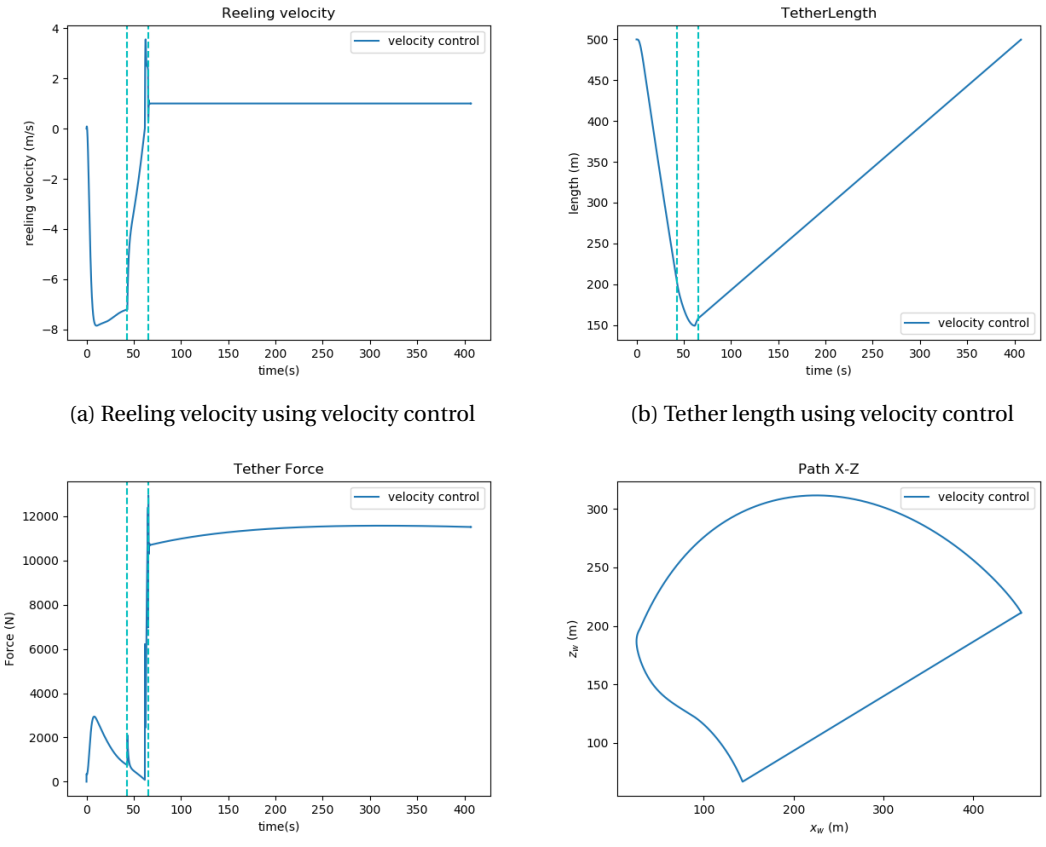

(a) Reeling velocity using velocity control

(b) Tether length using velocity control

(c) Tether force using velocity control

(d) Path using velocity control

Figure 6.6: Simulation full pumping using the ground station model, for (closed-loop) velocity control

In previous plots can be observed that during the retraction phase (1) the reeling velocity decreases quickly, overshoots the reference velocity a little, which is then compensated by the control. This results in a tether length which has a clear linear decreasing trend in the retraction phase from the moment the reeling veloc-

ity approaches its reference (negative) value. When the reeling velocity decreases in the retraction phase, the tether force increases, probably caused by an increase of apparent wind velocity when reeling-in fast. Once the reeling velocity stabilizes, the tether force shows a decreasing trend.

In the transition phase (2) the reeling velocity increases fast, but not with an infinite acceleration like in previous simulation with the basic settings. The first part of the transition phase is defined untill the moment the reeling velocity is 0 m/s. In this first part the tether length still decreases due to negative reeling velocity. Also the tether force decreases (except from a small peak), as a result of the increasing reeling velocity. In the second part of the transition phase the kite settings change, resulting in a quick increase in tether force. The tether force peaks but not as much as in the previous simulation with the basic settings. The increase in tether force also increases the reeling velocity quickly, making it overshoot the reference velocity. In the path of this simulation one can see the effect of the reel-in and reel-out part during the transition phase, making it a more smooth path compared to previous simulation.

During the traction phase (3) however, the control responds quickly, and the reeling velocity converges to its reference value. Also the tether force converges to a steady state and the tether length to a linear increasing trend.
The overall profiles of the reeling velocity, tether length and tether force of this simulation show similarities to the profiles of the experimental data. Improvements of this simulation in comparison to the simulation with basic settings are the following:

- The acceleration during the transition is not infinite. This causes a reel-in and reel-out phase during the transition phase, resulting in a smooth turn around between the retraction and the transition phase.

- The peak in tether force during the second part of the transition phase is lower.

6.2.4. Simulation using the ground station model and force control

Figure 6.7 shows a simulation of a full pumping cycle, using the ground station model and the (closed-loop) force control. The reference tether force is set to 1500 N during the retraction phase and to 9500 N during the second part of the transition phase and the traction phase. During the first part of the transition phase the velocity control is applied, setting the reference velocity to 0 m/s.

When looking at the tether force in subfigure 6.7c, one can see that the force control is indeed effective. During both the traction and the retraction phase the tether force converges to the reference value after some oscillations.
In the retraction phase (1) a decreasing trend in the reeling velocity can be observed in subfigure 6.7a. This is triggered by the force control. However, this decreasing velocity profile doesn't correspond well to the experimental data.

In the first part of the transition phase (2) the reeling velocity increases quickly causing a drop in the tether force. Once the reeling velocity is 0 m/s the kite changes settings and the force control makes the tether force increase quickly to the desired reference force. The tether force overshoots the reference force, but this time only a little peak is caused. In order to achieve high acceleration in the tether force, the reeling velocity gives a boost by turning in opposite direction.

In the traction phase (3) the tether force converges towards the reference force and also the reeling velocity converges to a steady state.
The path of this simulation has a smooth turn around point when going from retraction phase to transition phase.

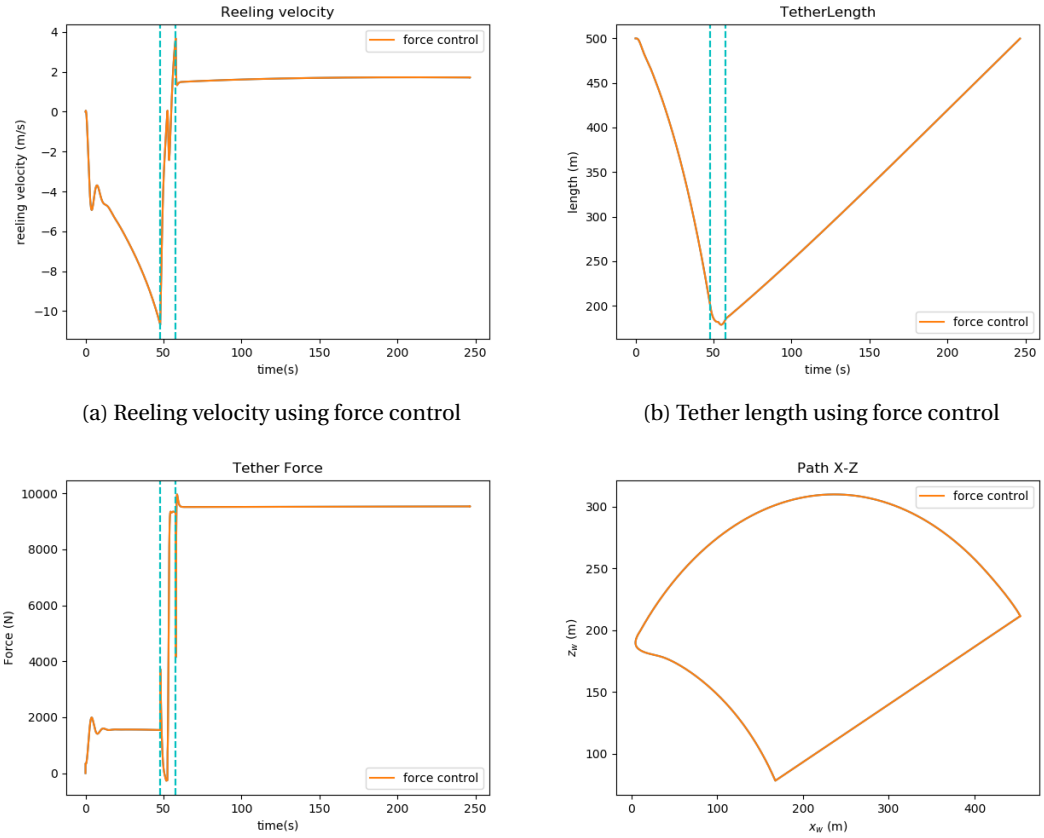

(a) Reeling velocity using force control

(b) Tether length using force control

(c) Tether force using force control

(d) Path using force controll

Figure 6.7: Simulation full pumping using the ground station model, for (closed-loop) force control

Although this simulation shows less similarities to the experimental data in comparison to the simulations using the velocity control, the behavior of the ground station can still be considered more physically realistic then the simulation with the basic settings. Mainly the finite acceleration of the reeling velocity during the transition phase is a big improvement. Also the low peak in the tether force, due to the force control, is more realistic. When an even smoother force control would be used, the tether force peak could die out even more. During an experiment the tether force is controlled, only when the force peaks too much. Probably the conditions during this experiment were not so extreme, and therefore it wasn't necessary to control the force. This could explain why the similarities between last simulation and the experimental data are not so big. Comparing the force control simulation to an extreme experiment, with strong wind gusts for example, might result in more similarities.

6.2.5. Comparing simulations

In figure 6.8 all three simulations are plotted. The first simulation, with the basic settings, is used as a baseline situation to see the improvements of the simulations using the ground station model.
When comparing all three simulations to the experimental data, the following improvement of the simulations using the ground station model can be observed in comparison to the simulation with the basic settings:

1. The acceleration of the reeling velocity during the transition phase finite in stead of infinite. Resulting in a smooth turn around point in the tether length and in the path between the traction and transition phase.

2. The peak in the tether force during the second phase of the transition phase is lower and can be controlled by the force control.

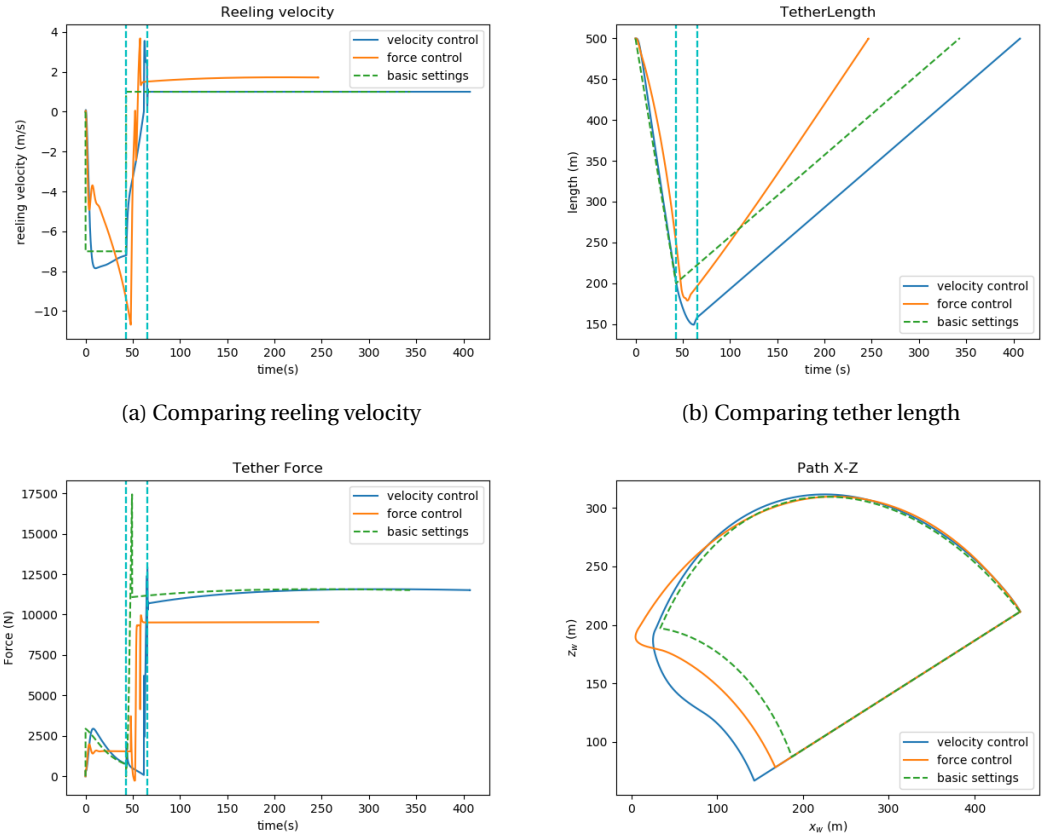

(a) Comparing reeling velocity

(b) Comparing tether length

(c) Comparing tether forcel

(d) Comparing Path

Figure 6.8: Comparing simulations of full pumping, using basic settings and the ground station model with velocity and force control

For this experiment, the simulations using the velocity control shows more similarities to the experimental data then the simulations with force control. This might be caused by the weather conditions of the experiment. Both the (closed-loop) velocity and force control trigger the desired behavior of the ground station in accordance to the reference values, although the controls could be more refined and better tuned. Probably a combination between the velocity and the force control would come closer to reality, since this combination is also incorporated in the real life ground station during experiments.

7

Conclusion and Recommendations

The research question of this thesis is the following:

> How can we mathematically model and control the Kitepower ground station
> in order to make physically realistic simulations?

A ground station model is derived, using physical principles of rotational mechanical systems, and by researching the behavior of all separate components of the ground station.
This led to the following mathematical model for the Kitepower ground station:

$$J\dot{\omega} = rF_t - b\omega - u \tag{7.1}$$

where the control u is determined by the transducer torque.
A rather simple but effective model. Refinements could be made in, for example, the transducer torque. It is now assumed that the transducer torque can be set, while in fact the generator and electrical motor are complex electrical machines. When 'setting' the torque, actually the integrated software of the generator/electrical motor makes the adjustments. Incorporating these adjustments in the model might make it more physically realistic.
Also, the radius and mass of the drum is assumed to be constant, while in real life this is not the case. Due to reeling-in and reeling-out the tether the radius and mass changes throughout each cycle. The changes are proportionally small, and therefore neglected in this thesis, but taking a time dependent radius and mass might improve the physical realistic behavior of the mathematical model.

For controlling the ground station during the simulations, the following updating formula of the (closed-loop) integral controls are proposed:

$$\begin{aligned} u_{k+1} &= u_k + h \cdot \lambda_v(\omega - \omega^{ref}), \\ u_{k+1} &= u_k - h \cdot \lambda_F(F_t - F_t^{ref}), \end{aligned}$$

where the first formula updates the *velocity control* and the second control the *force control*. Both controls satisfy the desired behavior according to a reference value, although they both oscillate to get to the desired state. For a higher λ value the control reacts faster, but also oscillates more.
Making the controls a *PID* control, by adding a Proportional and a Derivative term, would potentially improve them. However, a certain reference control value is then needed. In this thesis an open-loop control is derived, using *QMsimple*, which might function as a suitable reference control value. By using *QMcomplex* this reference (open-loop) control could be improved in further research.
For making physically realistic simulations, a closed-loop (feedback) control is recommended and not an open-loop control, since the ground station is also controlled using feedback in real life.

The ground station model and the controls are implemented in Python and incorporated in Kitepowers software, making it possible to perform simulations of full pumping cycles using *QMcomplex*. From those simulations it is clear that the ground station model indeed improves the physically realistic behavior of the simulation when comparing it to previous simulations, when using basic settings. Important improvements can be observed in the acceleration of the reeling velocity during the transition phase. This acceleration is now finite instead of infinite, meaning that the moment of inertia of the system is taken into account.
Comparing the simulations with the experimental data shows that the simulation using velocity control has more similarities to the experimental data than the one using force control. This might be caused by the weather conditions. Probably a combination of both controls would lead to even more physically realistic simulations.

For the implementation, the explicit Forward Euler method is being used to discretize the ground station model. An effective method, although other discretization methods, like implicit Euler or Runga Kutta might result in better approximations. This again could also improve the physically realistic behavior of the simulation.

Although both the ground station model and the control can still be improved in various ways, they are effective and improve the simulations of physically realistic behavior.

Bibliography

[1] Uwe Ahrens, Moritz Diehl, and Roland Schmehl. *Airborne wind energy*. Springer Science & Business Media, 2013.

[2] Junaid Alam, Hafsa Hassan, Sohaib Shamim, Waqas Mahmood, and Muhammad Sabieh Anwar. Precise measurement of velocity dependent friction in rotational motion. *European Journal of Physics*, 32(5):1367, 2011.

[3] A Batut. *La photographie a'erienne par cerf-volant. Gauthier-Villars et fils*. Paris, http://gallica.bnf.fr/ark:/12148/bpt6k1102849, 1890.

[4] Carnet de Vol. Wireless. `http://www.carnetdevol.org/Wireless/marconi-transatlantique.html`, 2013. Accessed 2013-06-25.

[5] Richard P Feynman, Robert B Leighton, and Matthew Sands. *The Feynman lectures on physics, Vol. I: The new millennium edition: mainly mechanics, radiation, and heat*, volume 1. Basic books, 2011.

[6] Kitepower. Kitepower about. `www.kitepower.nl`, 2018. Accessed: 2018-06-19.

[7] University of Michigan. Introduction: Pid controller design. `http://ctms.engin.umich.edu/CTMS/index.php?example=Introduction&section=ControlPID`, unknown. Matlab and Simulink.

[8] R.A. Serway and Jr.J.W. Jewett. *Physics for Scientists and Engineers*. 6th Ed. Brooks Cole, 2003.

[9] Michael Traut, Paul Gilbert, Conor Walsh, Alice Bows, Antonio Filippone, Peter Stansby, and Ruth Wood. Propulsive power contribution of a kite and a flettner rotor on selected shipping routes. *Applied Energy*, 113:362–372, 2014.

[10] Ton J.J. van den Boom. Introduction modeling and control. *Lecture Notes WB2104*, 2012.

[11] Rolf van der Vlugt, Anna Bley, Michael Noom, and Roland Schmehl. Quasi-steady model of a pumping kite power system. *CoRR*, abs/1705.04133, 2017.

[12] Wiki. Wiki how. `https://www.wikihow.com/Determine-Gear-Ratio`, 2018. Accessed: 2018-06-19.

A

Relevant Physical Concepts

In this section the physical concepts of rotational mechanical systems, relevant for deriving the ground station model, are briefly described. We start by defining some general symbols and their units.

Table A.1: General Symbols and Units

Symbol	Quantity	Unit symbol	Unit name
m	mass	kg	kilogram
v	velocity	$\frac{m}{s}$	meter per second
F	force	$N = \frac{kg \cdot m}{s^2}$	Newton
W	work	Joules	$J = Nm = \frac{kg \cdot m^2}{s^2}$
P	power	Watt	$\frac{Joules}{second}$
r	radius	m	meter
θ	rotation angle	rad	radians
ω	angular velocity	$\dot{\theta}$	$\frac{Radians}{second}$
α	angular acceleration	$\ddot{\theta}$	$\frac{Radians}{second^2}$
τ	torque	$N \cdot m$	Newton $\cdot$ meter
J	moment of inertia	$kg \cdot m^2$	kilogram meter squared

First rotations [5] will be discussed. Rotations can be described by the rotated angle (θ), the angular velocity (ω) and the angular acceleration (α). The rotated angle describes how many radians an object has rotated. The angular velocity describes how many radians per second an object rotates. Therefore the angular velocity is the derivative of the rotated angle with respect to time

$$\omega = \dot{\theta}.$$

This is analogous to velocity in linear motion (v), where velocity is the time derivative of the place (x), $v = \dot{x}$. The angular acceleration is the time derivative of the angular velocity, it describes the change of the angular velocity over time

$$\alpha = \dot{\omega} = \ddot{\theta}$$

With linear motion the linear acceleration (a) has a similar definition $a = \dot{v} = \ddot{x}$.
Now the rotation is defined, we're interested in the rotational force. This rotational force is called torque (τ), or moment force, and is determined by the force applied to the rotating object in tangential direction to the rotating motion (F_{tan}) and the distance of the point of application to this force to the rotating center (r). [8]. Torque is defined as follows:

$$\tau = F_{tan} \cdot r, \tag{A.1}$$

Anti-clockwise torque is considered to be positive, and clockwise torque negative. Negative torque is situated in the following figure.

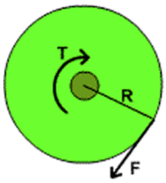

Figure A.1: torque

where in the figure $T = \tau, R = r$.

The famous 2^{nd} law of Newton states that the change of momentum (mv) is proportional to the force applied ($F = \frac{d}{dt}(mv)$). For a constant mass it follows that $F_{net} = m \cdot a$. For external torque the same idea holds, but then for an angular momentum which is defined as $J\omega$. Here J is the moment of inertia which represents the resistance of an object to change state in a circular moment. It is comparable to the effect of mass in a linear motion, and ω is analogous to the the velocity v. For the net torque (sum of all torques working on the system), the principle of Newtons 2^{nd} law can be applied to angular momentum which results in

$$\tau_{net} = \frac{d}{dt}(J\omega) \tag{A.2}$$

This is also known as the conservation law of angular momentum. When no net torque is applied to the system, the angular momentum remains constant.
When J is constant this conservation law can be simplified to

$$\tau_{net} = J\alpha = J\dot{\omega}. \tag{A.3}$$

How is the moment of inertia exactly defined? The moment of inertia depends on the mass of the rotating object, and how far this mass is placed from its rotating center. Let m_i be a mass particle with a distance d_i to the rotating center, then the definition of the moment of inertia is

$$J = \sum_i m_i d_i^2 \tag{A.4}$$

or, when integrating over all mass particles in the whole object (D)

$$J = \int_D d^2 dm \tag{A.5}$$

Let us now focus a bit longer on the net torque (τ_{net}). *Net* implies that there are more torques working on a system. This is possible when there are several external forces working on the system, and one of these external forces can be friction. Friction can be seen as a rotational damper and works proportional to the angular velocity. Based on paper [2], we assume that the resistive torque of friction varies linearly with the speed, and is always in opposite direction to the reeling velocity. Therefore friction torque (τ_{fr}) is defined as follows:

$$\tau_{fr} = -b\omega \tag{A.6}$$

The next thing to be discussed in this section is the relation between the angular velocity of the drum and the reeling velocity of the tether when reeled on or off the drum. The reeling velocity is also called the tangential velocity (v_t) and is determined by the angular velocity of the drum and by the radius of the drum. It is the distance covered by the circumference in meters per second. The reeling velocity can be calculated from the angular velocity

$$v_t = \omega r \tag{A.7}$$

With r the radius of the drum. Once the angular velocity and the radius of the drum are known, the reeling velocity is as well.

The last concept that will be briefly explained is the gearbox. Between the drum and the transducer a gearbox is situated. The gearbox in the ground station has a fixed gear ratio (G_r). A gear ratio is a direct measure of the ratio of the rotational speeds of two or more interlocking gears [12]. In our case we define the gear connected to the transducer as the driver gear, and the gear connected to the drum as the driven gear. The number of teeth of the driver gear will be denoted as T_1 and of the driven gear with T_2. The gear ratio is then defined as follows:

$$G_r = \frac{T_2}{T_1}$$

Meaning that when the drum goes around once, the transducer makes G_r rounds. Or more general:

$$\omega_1 = G_r \omega_2 \tag{A.8}$$

with ω_1 and ω_2 being the angular velocity of the driver and the driven gear respectively.

The generated power, which is defined as $P = \tau\omega$, should remain constant if we neglect the effect of friction on the changing angular velocity. Let P_1, τ_1 and P_2, τ_2 be the power and torque of the driver and the driven gear respectively, then

$$P_1 = P_2 \Rightarrow \tau_1\omega_1 = \tau_2\omega_2 \tag{A.9}$$

From this equation and equation A.8 now follows that

$$\tau_1 = \frac{1}{G_r}\tau_2. \tag{A.10}$$

This section was a brief introduction to rotational motion, torque, angular momentum, moment of inertia, friction, tangential velocity and the effect of a gearbox. In following table we summarize the most important aspects.

Table A.2: Summary of the relevant basic physical concepts

Concept	Formula
rotation angle	θ
rotational velocity	$\omega = \dot{\theta}$
rotational acceleration	$\alpha = \dot{\omega}$
torque	$\tau = F_{tan} r$
moment of inertia	$J = \sum_i m_i d_i^2$
conservation of angular momentum	$\tau_{net} = \frac{d}{dt}(J\omega)$
friction torque	$\tau_{fr} = -b\omega$
reeling velocity	$v_t = \omega r$
Gear ratio	$G_r = \frac{T_2}{T_1}$
Gear and angular velocity	$\omega_1 = G_r \omega_2$
Gear and torque	$\tau_1 = \frac{1}{G_r}\tau_2$